A Numerical Study on Phase Transformation and Hardness Evolution During Scanning Induction Hardening

M. Areitioaurtena, U. Segurajauregi, R. Hidalgo, I. Urresti, and E. Ukar

Abstract Induction hardening is a heat treatment that is frequently used to improve the mechanical properties of the surface of components typically subjected to contact loads, such as bearings or gears, extending component life. The simulation of the induction hardening process is very complex and time-consuming, which increases time-to-market in new industrial processes as the typical approach to define the induction hardening parameters is trial and error. In this work, we present a numerical study on the evolution of microstructural phases and hardness prediction for a complex industrial case, where the induction hardening process of a large-size pitch bearing is simulated. This kind of component is hardened by scanning, where there is relative movement between the inductor and workpiece and the inductor is followed by a quenching shower. Simulating scanning induction hardening is especially challenging as simultaneous heating and cooling occur, increasing the multiphysical interactions that must be simulated. The results show the evolution of the microstructure during induction heating and subsequent quenching accompanied by a prediction on the hardened case. A homogeneous hardened within the industrial span can be achieved in the workpiece after the combined static-scanning hardening is applied in the study.

Keywords Heat treatment · Large-size bearing · Process simulation · Scanning induction hardening · Coupled model · Multiphysics

M. Areitioaurtena (✉) · U. Segurajauregi · R. Hidalgo · I. Urresti
Ikerlan Technology Research Centre, Basque Research and Technology Alliance (BRTA), Paseo J.M. Arizmendiarrieta 2, 20500 Arrasate-Mondragon, Spain
e-mail: mareitioaurtena@ikerlan.es

E. Ukar
Department of Mechanical Engineering, University of the Basque Country, Alameda Urquijo S/N, 48013 Bilbao, Spain

G. Conte and O. Sename (eds.), *Proceedings of 10th International Conference on Mechatronics and Control Engineering*, Lecture Notes in Mechanical Engineering,
https://doi.org/10.1007/978-981-19-1540-6_1

1 Introduction

Induction hardening is a superficial heat treatment that is highly effective, integrable, quick, and non-contact and is usually applied to load-bearing and wear susceptible components. The required set-up for induction heating is very basic and requires the billet itself, a coil or inductor, and a source of current. The part is positioned near the inductor and heated by the eddy currents produced due to the electromagnetic phenomena [1]. The surface layer or other specific areas of the component are heated until the target areas are above austenization temperature A_3 and austenite is formed. Subsequent quenching is applied, usually by spraying water or aqueous polymers onto the hot surface or by immersion. The rapid cooling turns austenite into martensite, which is a microstructural phase that is much tougher and harder. The localized heating during induction hardening allows the core to remain ductile while a hard martensitic layer is reached on the surface. The hardened case depth and pattern can differ tremendously as they depend on the applied frequency current, which can range from 50 Hz to multiple megahertz, creating depths that can vary from less than one millimeter to the component's total volume in some cases.

The induction hardening process involves a variety of physics, which interact in a highly coupled way because the properties of the materials depend on several aspects, such as temperature and microstructure [2]. Due to its numerous and complex multiphysical interactions shown in Fig. 1, and the required vast amount of difficult-to-obtain data, the simulation of the induction hardening process has not been widely studied in academia, as these aspects increase computational time enormously, which leads to very little use of the current simulation tools in the industry. It is possible to test various process strategies and parameters (current intensity, frequency, power, scanning speed, and geometries) by simulating the induction hardening process,

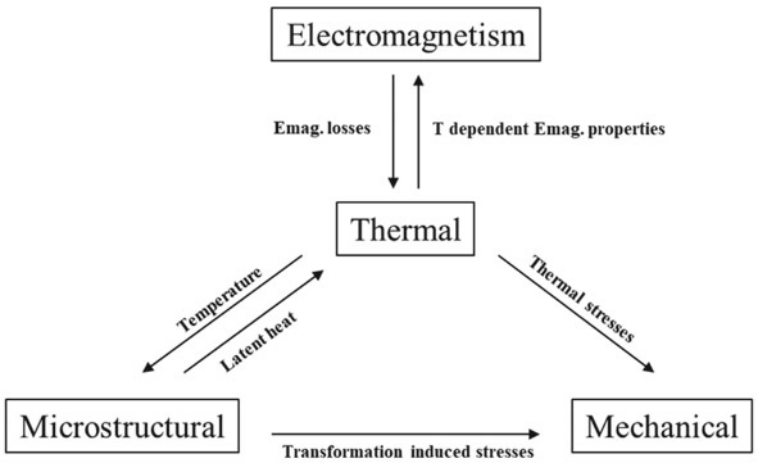

Fig. 1 Multiphysical interactions in induction hardening

in order to be able to predict final hardened case properties and also to determine possible process errors and failures, such as heating discontinuities, overheated areas, or cracking appearance, among others.

The electromagnetic–thermal coupling needs several back-and-forth iterations due to the sudden change in the electromagnetic properties of nonlinear ferromagnetic materials with temperature and is typically the coupling that requires the longest computational cycles, because electromagnetic simulation is extremely time-consuming.

Several published works have documented the simulation of the induction hardening process. A basic electromagnetic and thermal model is used in the work presented by Wrona et al. [3] to compute the evolution of temperature during the gear hardening by induction. Choi et al. [4] and Li et al. [5] carried out a similar analysis, where the prediction of the hardness profile in the cylindrical workpiece is included, achieving good agreement with experimental results. The research by Hömberg et al. [6] and Cajner et al. [7] show coupled models where microstructural transformations and hardness are computed and experimentally validated in spur-gears and discs and 42CrMo4 cylinders, respectively.

In this work a completely coupled electromagnetic-thermal-metallurgical-mechanical model is presented along an industrial case study, demonstrating that the developed model can be used to compute complex three-dimensional cases with adequate computational time, predicting the pattern and hardness values of the hardened case and its microstructure.

2 Modeling Scanning Induction Hardening

A fully coupled electromagnetic-thermal-microstructural-mechanical model is required for the simulation of the simultaneous scanning induction hardening process. In this work, the ANSYS commercial software has been used. The software is currently unable to compute microstructural transformations, but these can be incorporated into the model by implementing the constitutive equations into subroutines or using the software's own coding language, Ansys Parametric Design Language (APDL).

2.1 Electromagnetic-Thermal Coupling

A semi-analytical strategy has been used in this work to solve the electromagnetic coupling, as used in a previous work by the authors [8]. The usage of the semi-analytical approach brings shorter computational times than commercial dedicated softwares, especially for complex industrial cases where a three-dimensional computation is usually required. First, the electromagnetic solver resolves the diffusion Eq. (1) computed from Maxwell's equations. The computed magnetic field strength

is introduced into an analytical model that, combined with a thermal FE model, is able to calculate the heat generation caused by the induced currents and the resulting temperature distribution, by resolving the heat Eq. (2).

$$\sigma \frac{\partial \boldsymbol{A}}{\partial t} - \frac{1}{\mu}\nabla^2 \boldsymbol{A} = \boldsymbol{J}_S \tag{1}$$

$$\rho c_P \frac{\partial T}{\partial t} - \nabla(\kappa \nabla T) = \dot{q} \tag{2}$$

Further details of the semi-analytical approach and electromagnetic material properties can be found in Ref. [8].

2.2 Microstructure

During induction heating, γ austenite is generated when the temperature reaches the critical austenitization temperature range, where the initial microstructure is transformed between the austenite start and end temperatures (AC_1 and AC_3, respectively). For 42CrMo4, the critical temperatures that have been used in this work are 759 and 805 °C. Equation (3) can be used to describe the volumetric fraction of transformed austenite during heating [9].

$$f_\gamma = 1 - \exp\left(k \frac{AC_1 - T}{AC_1 - AC_3}\right) \tag{3}$$

The Johnson–Mehl–Avrami–Komogorov model, also known as JMAK model, describes the parent austenite decomposition into daughter phases when the transformation is considered diffusive, such as for the case of α ferrite, P pearlite, or α_b bainite, denoted as phase i in Eq. (4)

$$f_i(T,t) = 1 - exp\left[-b(T)t^{n(T)}\right] \tag{4}$$

where parameters $b(T)$ and $n(T)$ depend on the kinematics of each microstructural phase and are computed from the TTT diagram (these equations can be found in Ref. [10]).

Martensitic (α') transformation, which is the main microstructural phase generated during quenching, can be computed by Koistinen and Marburger Eq. (5).

$$f_{\alpha'}(T,t) = 1 - exp[-0.011(M_S - T)] \tag{5}$$

The critical temperatures for austenite and martensite transformations have been described by several analytical equations and depend on the chemical composition of the material.

Table 1 Chemical composition ranges of 42CrMo4 specified by standard EN 10083-3

	C	Mn	P	S	Si	Cr	Mo
Min	0.38	0.6	–	–	–	0.9	0.15
Max	0.45	0.9	0.025	0.035	0.4	1.2	0.3

$$A_1 = 723 - 10.7\,\mathrm{Mn} - 16.9\,\mathrm{Ni} + 29\,\mathrm{Si} + 16.9\,\mathrm{Cr} + 290\,\mathrm{As} + 6.4\,\mathrm{W} \quad (6)$$

$$A_3 = 912 - 203\sqrt{\mathrm{C}} - 15.2\,\mathrm{Ni} + 44.7\,\mathrm{Si} + 104\,\mathrm{V} + 31.5\,\mathrm{Mo} + 13.1\,\mathrm{W} + 30\,\mathrm{Mn} - 11\,\mathrm{Cr} - 20\,\mathrm{Cu} + 700\,\mathrm{P} + 400\,\mathrm{Al} + 120\,\mathrm{As} + 400\,\mathrm{Ti} \quad (7)$$

$$M_S = 561 - 474\,\mathrm{C} - 33\,\mathrm{Mn} - 17\,\mathrm{Ni} - 17\,\mathrm{Cr} - 21\,\mathrm{Mo} \quad (8)$$

The chemical composition of 42CrMo4 is specified by standard EN 10083-3. Typical values for 42CrMo4 are shown in Table 1.

A Time–Temperature–Transformation diagram (known as TTT diagram) is shown in Fig. 2, computed using the upper limits of the chemical composition of the steel specified by the standard.

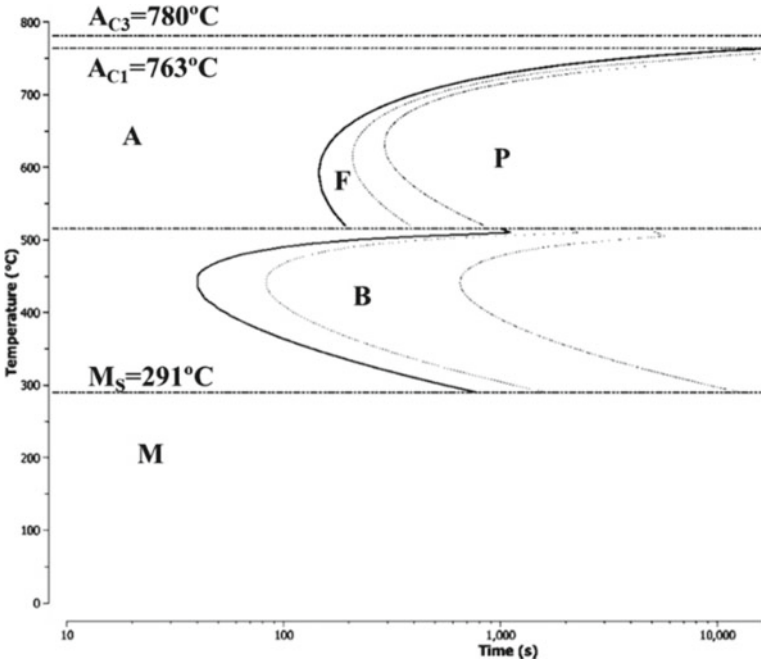

Fig. 2 Time–Temperature–Transformation diagram for 42CrMo4

2.3 Hardness

Vickers Hardness can be evaluated from the chemical composition of the material. Each microstructural phase has a specific hardness and a linear rule of mixture can be used to compute the hardness based on the fraction of microstructural phases and their hardness values.

$$HV_{\mathrm{M}} = 127 + 949\,\mathrm{C} + 27\,\mathrm{Si} + 11\,\mathrm{Mn} + 8\,\mathrm{Ni} + 16\,\mathrm{Cr} + 21\ln V_r \tag{9}$$

$$\begin{aligned} HV_{\mathrm{B}} = &-323 + 185\,\mathrm{C} + 330\,\mathrm{Si} + 153\,\mathrm{Mn} + 65\,\mathrm{Ni} + 144\,\mathrm{Cr} + 191\,\mathrm{Mo} \\ &+ (89 + 53\,\mathrm{C} - 55\,\mathrm{Si} - 22\,\mathrm{Mn} - 10\,\mathrm{Ni} - 20\,\mathrm{Cr} - 33\,\mathrm{Mo})\ln V_r \end{aligned} \tag{10}$$

$$\begin{aligned} HV_{\mathrm{F,P}} = &42 + 223\,\mathrm{C} + 53\,\mathrm{Si} + 30\,\mathrm{Mn} + 12.6\,\mathrm{Ni} + 7\,\mathrm{Cr} + 19\,\mathrm{Mo} \\ &+ (10 - 19\,\mathrm{Si} + 4\,\mathrm{Ni} + 8\,\mathrm{Cr} + 130\,\mathrm{V})\ln V_r \end{aligned} \tag{11}$$

where V_r denotes the cooling rate at 700 °C and chemical elements are introduced in weight percentage.

3 Case Study: Large-Size Bearings

Pitch bearings play an important role in the operation of wind turbines, as they are able to connect the blades to the rotor while allowing the orientation change that is required depending on the wind direction, speed, or force. In the most common wind turbines that are currently in operation, the diameter of pitch bearings varies up to 3 m, with a typical construction of a four-point contact double-row ball bearing, as shown in Fig. 3 (left). Their races are typically hardened by induction because of the mechanical requirements for these parts, with a standard hardening depth of approximately 5–7 mm. A common technique for hardening the races is to conduct the induction hardening operations separately for each race. Due to their large size, pitch bearings must be hardened by scanning, where there is a relative movement between the inductor and the workpiece.

As the races are hardened separately, it is possible to consider that a single row can be computed based on the hypothesis that 1: there is enough time for the area to cool down to room temperature before heating the second race and 2: the heat generated in the second race does not affect the microstructure of the already hardened race as the distance between hardened cases is sufficient, thus, not creating a self-tempering of the first race.

Because of the large diameter of the bearing, the area of study has been considered straight for the sake of simplicity. For the initial static electromagnetic simulation, a double-turn inductor is used, along a flux concentrator that allows more efficient

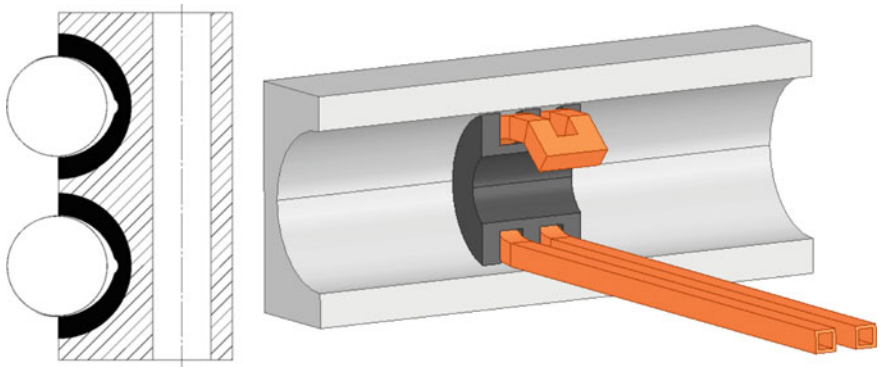

Fig. 3 Cross-section of a double row ball bearing (left) and electromagnetic model including inductor and field concentrator (right)

usage of the machine power—thus, improving power consumption and opening the possibility to use less powerful machines. The air must also be included in the electromagnetic FE simulation, giving a total of 100 k elements. For the subsequent coupled thermal-metallurgical-mechanical simulation, only the workpiece is modeled using 390 k elements, where the surface and subsurface areas have a very fine mesh in order to use the developed semi-analytical electromagnetic-thermal approach. Induction parameters are 20 kHz and 2100 A (RMS value) and the scanning speed is set to 3.5 mm/s. During the scanning process, the inductor is followed by a shower that projects an aqueous polymer that cools the hot surface fast enough to generate the martensitic layer. For the developed model, the shower is modeled as a "cooling box," where a high convection coefficient (15,000 W/m^2K) is placed in selected moving areas. The cooling box is placed with a separation of 20 mm from the inductor with a width of 20 mm. The total process time was set to 30 s and the typical computational time for the coupled simulation was 3 h using 8 cores on a server equipped with Intel® Xeon® Gold 6242 CPU dual-processor (2.8 GHz) and 512 Gb RAM.

Figure 4 shows the evolution of the austenitized region during the scanning process and the martensitic layer after quenching. In the figure, it can be observed that the austenite is fully transformed into martensite, obtaining a hardened layer of approximately 5–8 mm depth, the maximum hardness being 860HV.

The results show that 12 s are required for the system to reach homogeneous austenitization temperatures through the cross-section. Thus, an approximate length of 42 mm, which corresponds to the approximate width of the inductor, will remain unhardened using the proposed hardening strategy, which is usually called soft spot or soft zone. In order to reduce or totally avoid soft zones, one can find several patented techniques using one or more inductors.

One of the main results that are critical for service life is the residual stress pattern obtained after induction hardening. Further development of the presented model will include the prediction of residual stresses after the heat treatment, as it has been

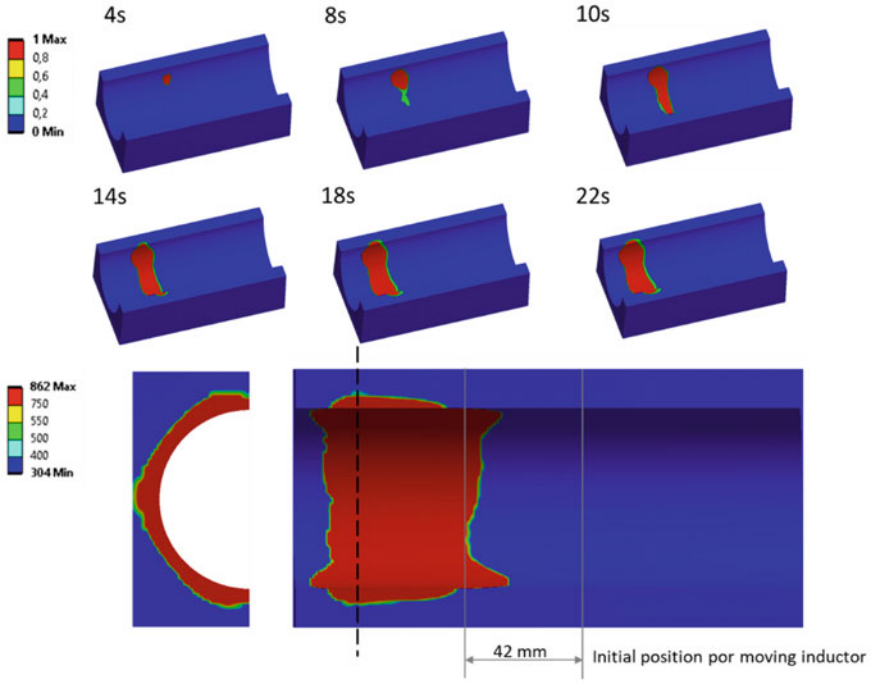

Fig. 4 Austenite evolution during scanning induction hardening (above) and hardness layer in workpiece and cross-section after 30 s (below)

demonstrated that compressive residual stresses on surface and subsurface areas slow down crack propagation, extending component life.

4 Conclusions

A coupled electromagnetic-thermal-metallurgical-mechanical model was presented in this paper for the numerical simulation of the scanning induction hardening process in complex industrial cases, which brings the possibility of carrying out extensive numerical analyzes in the industrial context, possibly reducing time-to-market and very high costs associated with the process definition developments.

The developed model was applied to an industrial-based case study, where the scanning induction hardening of large-size pitch bearings was simulated, obtaining expected results for microstructure and hardened depth and case pattern. In this field, it is of great importance to achieve an efficient and favorable process as structural integrity is highly affected by the results of the induction hardening process and can be critical for service life.

Acknowledgments Ikerlan's research has been supported by CDTI, depending by Ministerio de Ciencia e Innovación, through the "AYUDAS CERVERA PARA CENTROS TECNOLÓGICOS 2019" program, project MIRAGED with expedient number CER-20190001. This research center is certificated as CENTRO DE EXCELENCIA CERVERA.

References

1. Rudnev V, Loveless D, Cook RL (2017) Handbok of induction heating
2. Şimşir C (2014) Modeling and simulation of steel heat treatment—prediction of microstructure. Distortion, Residual Stress, Crack ASM Handb 4B:409–466
3. Wrona E, Nacke B, Resetov D (2003) 3D-modelling of the transient eating process for induction surface hardening MEP-international scientific colloquium modelling for electromagnetic processing, pp 119–123
4. Choi JK, Park KS, Lee SS (2018) Prediction of high-frequency induction hardening depth of an AISI 1045 specimen by finite element analysis and experiments. Int J Precis Eng Manuf 19(12):1821–1827
5. Li H, He L, Gai K, Jiang R, Zhang C, Li M (2015) Numerical simulation and experimental investigation on the induction hardening of a ball screw. Mater Des 87:863–876
6. Hömberg D, Liu Q, Montalvo-Urquizo, Nadolski D, Petzold T, Schmidt A, Schulz A (2016) Simulation of multi-frequency induction hardening including phase transitions and mechanical effects Mater Des 121:86–100
7. Cajner D, Smoljan B, Landek D (2004) Computer simulation of induction hardening. J Mater Process Technol 157–158:55–60
8. Areitioaurtena M, Segurajauregi U, Urresti I, Fisk M, Ukar E (2020) Predicting the induction hardened case in 42CrMo4 cylinders. Procedia CIRP 87:545–550
9. Xia J, Jin H (2018) Numerical modelling of coupling thermal metallurgical transformation phenomena of structural steel in the welding process. Adv Eng Softw 115:66–74
10. Carlone P, Palazzo GS (2011) Development and validation of a thermomechanical finite element model of the steel quenching process including solid-solid phase changes. Int Appl Mech 46(8):995–971